FABRICATION, 3D FINITE ELEMENT ANALYSIS AND CHARACTERIZATION OF AN OPTICAL PASSIVE MICROSENSOR

Braggio Luciano[a] and Guarnieri F. Ariel[a,b]

[a]*Centro Internacional de Métodos Computacionales en Ingeniería (CIMEC), CONICET*
Email: luciano.braggio@gmail.com

[b]*Universidad Nacional de Entre Ríos – Facultad de Ingeniería – Carrera de Bioingeniería*
http://www.bioingenieria.edu.ar

Keywords: 3D, Diffraction Grating, FEM, PDMS, Soft Lithography

Abstract. In this work we present the 3D Finite Element Analysis (FEA) of an optical passive microsensor for measuring pressure in biofluids and the simulation of the required characterization setup. Previously, we reported the design and analysis of a prototype where simulations were performed by using the Finite Element Method (FEM) in order to analyze the mechanical behavior of the grating; the results were exported to an optical software for diffraction analysis. The microsensor is based on a deformable diffraction grating made of an elastomeric polymer (PDMS); as the PDMS membrane containing the diffraction grating is subjected to a pressure, its optical properties are varied and an indirect measurement of the pressure is attainable. Now, we report the fabrication and characterization of the optical passive microsensor. The simulation of the setup required for characterization brings many advantages as it enables a rapid understanding of the optical properties of the microsensor without implementing it. Therefore, a correct model of both the optical and the mechanical model accelerates the development-time of the prototype so as to carry out possible re-designs in the future.

1 INTRODUCTION

The micro-electro-mechanical-systems (MEMS) designed for the use in medicine and biological applications (BioMEMS) are devices fabricated with similar techniques as those for MEMS, but with the main purpose of being biocompatible (Grayson et al., 2004). Such devices are of particular interest in biomedical and biological areas where a miniaturized system is required, e.g. biosensors and microactuators that could be integrated and implantable. In the case where optical elements are also employed the devices are known as micro-opto-electro-mechanical systems (MOEMS). In the last years, MOEMS have been developed for monitoring local pressure in situations where both sensitivity, precision, minimal impact on the system to be studied, and reduced size are needed. Measurement of local pressure is of fundamental importance in flow characterization in microfluidic devices and many different physical principles were employed to achieve this goal. Optical passive monitoring of pressure is an interesting method because it allows real-time and remote sensing without the need of powering the sensor. An optical microsensor also has, if properly designed, excellent sensitivity and high-precision which are very desirable features of a transducer in these particular areas.

In a previous work, we presented the design and simulation of a pressure sensor based on a PDMS diffraction grating (Braggio and Guarnieri). This prototype was simulated using an opto-mechanical model in the pressure range of interest. The PDMS deformable diffraction grating showed to be a useful device for monitoring local pressure. Here we report the fabrication and characterization of this PDMS grating, aimed to work as an optical passive pressure sensor. Both simulations of the mechanical and optical model were performed. In the case of the mechanical model, many variations have been carried out with respect to our previous work. A hyperelastic model was used to describe the stress-strain relationship of the PDMS grating and the results from this model were compared with the linear elastic model and experimental data. These results were then used in the optical simulation. The outcomes obtained from simulations were compared with the measurement of the mechanical properties of PDMS carried out by Tae Kyung Kim et.al and with those achieved by our experiment (Kim et al., 2011).

The main purpose of this article was to advance in the understanding of the mechanical and optical properties of PDMS to be used as an optical passive pressure microsensor. It was also intended to validate the coupled opto-mechanical model for future applications in the design of the device. The present work is composed of seven sections. First, the design and working principle of the microsensor is briefly described. In section 2 the theoretical aspects of the optical and mechanical models are presented; sections 3 and 4 describe the fabrication of the microsensor and the simulations that were performed, respectively. Section 5 explains the characterization procedure that was carried out, whereas section 6 presents the results obtained. The last two sections submit the discussion and conclusions of the work.

1.1 Design and Working Principle

The device consists of a binary phase surface-relief grating embedded on a 100 micrometer-thick section of PDMS. The grating is of the transmissive-type. It has a rectangular shape and its pattern consists in a series of parallel equidistant grooves at a given period. This period is known as the *pitch* of the grating. In Fig. 1 a schematic of a typical surface-relief diffraction grating is shown. The height of the grooves is d_g , the pitch is λ and the width of the grooves is $f\Lambda$. The thickness of the substrate is denoted by d_w and the refractive indices of the air, the grooves and the substrate as n_L, n_H and n_W, respectively.

The operating principle of the detector is based on the optical changes that undergo in the
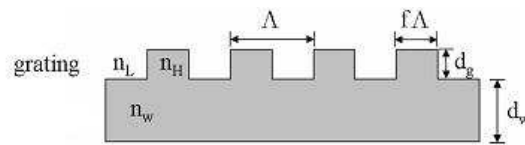
Figure 1: Schematic representation of a diffraction grating.

diffraction grating, as it is subjected to strains. These mechanical deformations have consequences on the pitch of the diffraction grating and as the pitch varies, it causes a shift in the angular positions of light beams deviated from the optical sensor. In the next section, the physical explanation of a diffraction grating is presented. In the absence of mechanical deformation (better expressed as strain), the grating has a nominal pitch. When incident light with a particular wavelength reaches the grating it is deviated into a series of beams at different angles. This diffraction pattern has no change if the optical properties of the grating are maintained and the wavelength of the light remains constant. At a certain distance from the grating, each particular light spot (diffraction mode) has a defined distance to the central one ($0 - mode$). As the grating is subjected to strain the pitch varies and there is a shift in the original diffraction pattern. Therefore, there is an indirect measure of the applied mechanical stress in the grating.

The microsensor consists of the following major blocks: a substrate, where the grating is embedded, and the diffraction grating itself. As it can be seen, the fundamental blocks of the device are very simple, but an excellent comprehension of the transducer is of fundamental importance to design and develop a proper sensor. Both the substrate and the grating are made of the same material. The microsensor offers the desired features: it is of simple fabrication, has a very good sensitivity, and it is made of a material with excellent properties for both optical and biomedical applications. In summary, the deformable PDMS diffraction grating is the pressure transducer and the deviated (diffracted) beams indicate changes in the applied pressure.

1.2 THEORY

1.2.1 Optical Model

A transmission or transmissive phase grating is a diffraction grating that consists of an array of diffracting elements that produces a periodic alteration in the phase of the emerged wave (Hecht, 2002). When monochromatic light is incident on a grating surface, it is diffracted into discrete directions and in fact there is a unique set of discrete angles where the beams can be seen, zones where the light interferes constructively (Palmer and Loewen, 2005). In the case of incident light with a wavelength of λ and a pitch d (distance between any two consecutive grooves as said before) the diffracted beams appear at angular locations determined by the grating equation (Eq. (1):

$$\sin(\theta) - \sin(\theta_0) = \frac{m\lambda}{d} \tag{1}$$

where θ is the angle of diffraction for the *mth-order* beam, θ_0 is the angle of incidence of the probing beam. This equation expresses the fact that if the parameters remain unchanged, the diffraction pattern is unaltered. In Fig. 2 a typical diffraction pattern of a transmission grating is shown. The diffraction angles are measured from the grating normal.

If the angle of incident light is zero and the distance from the diffraction grating to the plane
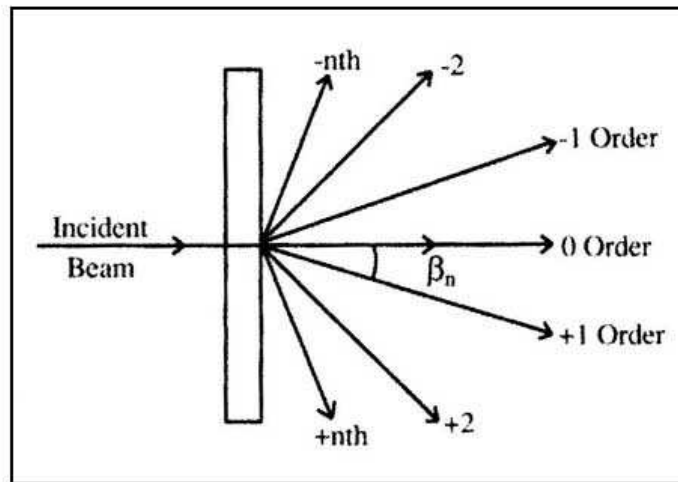
Transmission Grating Diffracted Orders

Figure 2: Diffraction pattern of an incident beam of light produced by a transmission grating.

of detection is much greater than the pitch of the grating, then the following equation holds:

$$y \approx \frac{m\lambda D}{d} \tag{2}$$

Where y is the vertical distance of the *m-th* diffracted beam measured at the plane of detection, D is the distance from the grating to the detector-plane and d is the pitch of the grating. The latter equation is the one that explains the working principle of the microsensor. If the pitch is a function of the mechanical stress prescribed on the PDMS grating, then as the pitch value decreases the diffraction pattern becomes wider.

1.3　Mechanical Model

In order to simulate the mechanical behavior of the microsensor a two parameters Mooney-Rivlin model was used. This one is suitable for modeling nearly incompressible hyperelastic materials such as PDMS. As a common knowledge, one of the most widely used models for such a material is the Mooney–Rivlin (MR) constitutive model (Yu and Zhao, 2009b). Many other hyperelastic models have since been developed (Kim et al., 2011). A model such as the MR is suitable for materials that are isotropic, highly elastic and incompressible under the condition of relatively high strain rate (Dong et al., 2005).

A hyperelastic material is defined by its strain energy function W_s, which is a function of the strain state. For an isotropic material, the strain energy function depends only on the invariants of the Cauchy-Green tensor as shown in the following equation:

$$\begin{aligned}
\mathbf{W}_s &= \mathbf{W}_s\left(\boldsymbol{I}_1, \boldsymbol{I}_2, \boldsymbol{I}_3\right) \\
\boldsymbol{I}_1 &= trace(\boldsymbol{C}) = C_{11} + C_{22} + C_{33} \\
\boldsymbol{I}_2 &= \frac{1}{2}(\boldsymbol{I}_1^2 - trace(\boldsymbol{C}^2)) \\
\boldsymbol{I}_2 &= \det(\boldsymbol{C}) = J^2
\end{aligned} \tag{3}$$

In the case of nearly incompressible materials, the strain energy function can be separated in two parts as expressed in equation 4. The first term is function of the modified invariants $\bar{I}_1$ and $\bar{I}_2$ that have no dependency on the volumetric effects, whereas the second part of the equation corresponds to the volumetric energy function shown in equation 5.

$$\mathbf{W}_s = \mathbf{W}_s\left(\bar{\boldsymbol{I}}_1, \bar{\boldsymbol{I}}_2\right) + U(J) \tag{4}$$

$$U(J) = \frac{1}{2}\kappa(J-1)^2 \tag{5}$$

$$\bar{\boldsymbol{I}}_1 = \boldsymbol{I}_1 J^{-\frac{2}{3}} \quad \bar{\boldsymbol{I}}_2 = \boldsymbol{I}_2 J^{-\frac{4}{3}} \tag{6}$$

Because of the mixed formulation used in the model, the hydrostatic pressure becomes a dependent variable which is derived from:

$$p = -\frac{\partial U}{\partial J} \tag{7}$$

Finally, the strain energy function $\boldsymbol{W}_s$ for the Mooney Rivlin model is shown in equation 8.

$$\mathbf{W}_s = C_{10}(\bar{\boldsymbol{I}}_1 - 3) + C_{01}(\bar{\boldsymbol{I}}_2 - 3) - p(J_{el} - 1) - \frac{p^2}{2\kappa} \tag{8}$$

Then, the strain energy function of this model is only a linear function of the modified invariants $\bar{\boldsymbol{I}}_1$ and $\bar{\boldsymbol{I}}_1$ and the pressure.

1.3.1 Determination of Mooney-Rivlin Coefficients

In order to calculate the coefficients of the MR models, a mathematical approach was done. As said before, there are two coefficients that need to be determined in the model and their values can be derived from the uniaxial experimental test.

If the right Cauchy-Green deformation tensor $\boldsymbol{C}$ is considered, the Green strain tensor is defined by the following relationship:

$$\boldsymbol{E} = \frac{1}{2}(\boldsymbol{C} - \boldsymbol{I}) \tag{9}$$

The second Piola–Kirchhoff stress tensor S can be expressed as:

$$\boldsymbol{S} = \frac{\partial \boldsymbol{W}}{\partial \boldsymbol{E}} = 2\frac{\partial \boldsymbol{W}}{\partial \boldsymbol{C}} \tag{10}$$

With the intention of simplify further calculations, the coordinate directions could be aligned with the principals directions of deformation; then the Cauchy strain tensor becomes:

$$\boldsymbol{C} = \begin{pmatrix} \lambda_1^2 & 0 & 0 \\ 0 & \lambda_2^2 & 0 \\ 0 & 0 & \lambda_3^2 \end{pmatrix} \tag{11}$$

Therefore, the invariants of $\boldsymbol{C}$ become:

$$\begin{aligned} \boldsymbol{I}_1 &= \lambda_1^2 + \lambda_2^2 + \lambda_3^2 \\ \boldsymbol{I}_2 &= \lambda_1^2\lambda_2^2 + \lambda_2^2\lambda_3^2 + \lambda_3^2\lambda_1^2 \\ \boldsymbol{I}_3 &= \lambda_1^2\lambda_2^2\lambda_3^2 \end{aligned} \tag{12}$$

The classic uniaxial and equibiaxial tensile tests can also be used for the characterization of a polymeric material with similar results as those carried out with more sophisticated facilities (**?**).

A uniaxial tensile test can be used in conjunction with analytic procedure to determine the critical material parameters of the MR hyperelastic model. For a special case of uniaxial tension, $\lambda_1 = \lambda, \lambda_2 = \lambda_2 = \lambda^{-\frac{1}{2}}, \sigma_{11} = \sigma, \sigma_{22} = \sigma_{22} = 0$ and the stress-strain equation can be expressed as (Yu and Zhao, 2009b; Dong et al., 2005):

$$\sigma_{UT} = \sigma_{11} = 2C_{10}(\lambda^2 - \frac{1}{\lambda}) + 2C_{01}(\lambda - \frac{1}{\lambda^2}) \tag{13}$$

Where σ_{UT} is the true stress in the uniaxial tension test and σ_{11} is the Cauchy Stress tensor in the principal direction.

As seen in equation 13, the coefficients of MR model are unknown and we need to impose two conditions in order to calculate them. The first condition is that for the MR-model to be consistent with its linear counterpart, at small strains i.e. the slope must equal the Young's modulus in the linear elastic model. The second condition is imposed by giving a defined stress value at the maximum strain at which the sample is submitted. Finally, the following system of linear equations is derived from which C_{10} and C_{01} can be computed:

$$
\begin{aligned}
\sigma_{11} &= -\left(\frac{1}{\lambda} - \lambda^2\right)\left(2\,c_1 + \frac{2\,c_2}{\lambda}\right) \\
\frac{\partial \sigma_{11}}{\partial \lambda} &= \left(2\,c_1 + \frac{2\,c_2}{\lambda}\right)\left(2\,\lambda + \frac{1}{\lambda^2}\right) + \frac{2\,c_2\left(\frac{1}{\lambda} - \lambda^2\right)}{\lambda^2}
\end{aligned}
\tag{14}
$$

The system of equation results in:

$$
\begin{aligned}
0 &= 6\,c_1 + 6\,c_2 - \frac{1}{4} \\
0 &= \frac{387\,c_1}{100} + \frac{387\,c_2}{160} - \frac{3}{16}
\end{aligned}
\tag{15}
$$

2 MATERIALS AND METHODS

2.1 Fabrication

A detailed explanation of the fabrication process is far beyond the scope of this work; however the steps followed in the fabrication and in particular the materials and masks used are presented here.

The technique followed for the construction of the PDMS microsensor is the replica molding method. This method belongs to what in general is known as soft lithography technique and is a rapid-prototyping technique where a mold or stamp is replicated from a master using an elastomer as key-material. A detailed explanation of this method can be found in the review from Xia and Whitesides among other soft lithographic techniques (Wilbur et al., 1996; Xia and Whitesides, 1998). Fig. 3 shows a simplified flowchart of the method.

The process begins with the design of the pattern to transfer. By mean of a mask, the pattern is transferred to a photosensitive material. This technique is known as projection photolithography. The mask was projected, i.e. the dimensions were reduced, onto a resist-coated glass substrate which was 30 [mm] in diameter. A negative photoresist (maN-1405 - Microchem) was used (Corning).

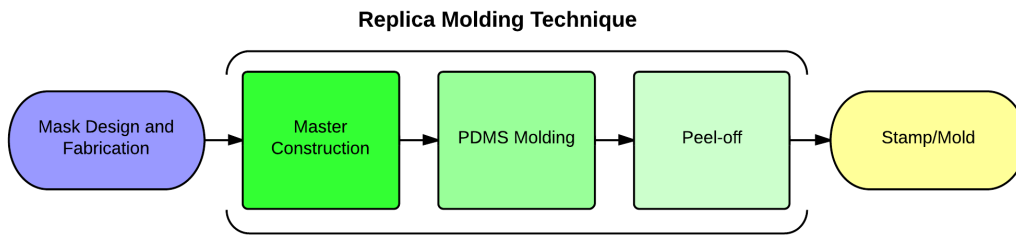**Replica Molding Technique**

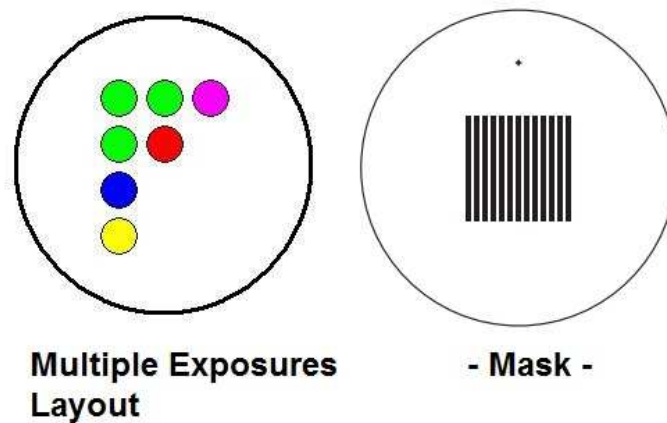Figure 3: Summarized flowchart of the Replica Molding Technique.

Figure 4: Schematic diagram of multiple exposures and Photolithographic Mask used in the fabrication of the grating.

Fig. 4 shows the mask designed and used for the construction of the PDMS grating. In the figure, at the left it is depicted with colors the different exposure doses used by the UV incident light, being the green-colored circles the calculated optimal dose and the other variations of it.

Once the master was created, PDMS in a 10:1 base polymer/curing agent mixing ratio was poured onto the master and baked in a hot-plate at a temperature of $70[^{o}C]$ for 25 minutes. Finally, the PDMS was cut and peeled off from the substrate in order to obtain the strips that then were characterized.

2.1.1 Poly-dymethil-siloxane (PDMS)

As said before, the microsensor is fabricated using PDMS as key material. PDMS is a kind of rubber-like material with nearly or purely incompressible property. PDMS is used because of its outstanding properties, such as low price, optical transparency, biocompatibility, and flexibility. PDMS is an elastomer with excellent properties that can be deformed reversibly and repeatedly without residual distortion. It is thermally stable, inexpensive, nontoxic, and commercially available (Yoon et al., 2010; Keum et al., 2012). PDMS has proven to be an exceptional material for micro-technology (Hosokawa and Maeda, 2001). Values of Young's modulus for PDMS
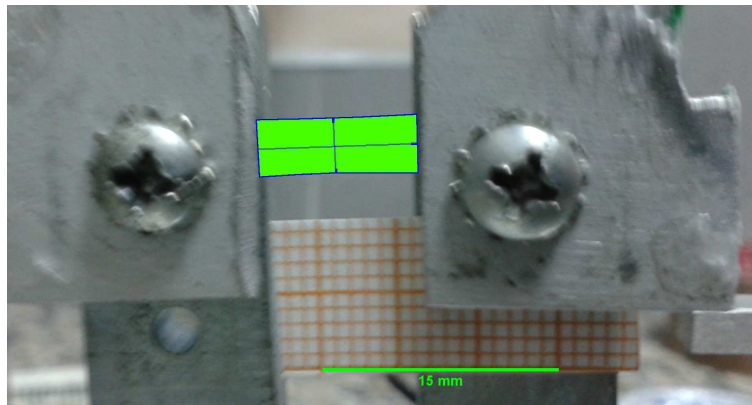
Figure 5: Processed photograph of the undeformed PDMS sample in the uniaxial tension test.

have been reported from around 0.35 to $3[MPa]$ (Foland et al., 2011). Micro-devices made from PDMS are easy to fabricate using the replica moulding technique (Schueller et al., 1999; Wilbur et al., 1996; Xia and Whitesides, 1998). PDMS has many features which makes it an excellent material for a pressure sensor, e.g. good biocompatibility, nontoxic and optically transparent (Chronis et al., 2003), easily fabricated and widely used in micro-fluidic devices (Yu and Zhao, 2009a). PDMS might be used as a biomedical material due to its excellent aspects like microfabricability, biocompatibility, and robust functionality. The major advantages of PDMS can be found in its fabrication process and material properties, as it was shown before.

3   SIMULATION

3.1   Mechanical Model

Mechanical simulation of the device was performed using a Finite Element Analysis (FEA) software. The entire sample was simulated in 3D mechanical model and both a linear elastic and a non-linear model were performed in order to compare the simulation with the experimental results. In the case of the non-linear model, a mixed-formulation was used because of the nearly-incompressibility of the PDMS. A mixed U-P (displacement-pressure) formulation allows element matrices to be formed using mixed variational principles with the pressure introduced to enforce the incompressibility constraint. It is applicable to nearly incompressible rubber-like materials with arbitrarily large displacements and strains.

3.1.1   Geometry of the model

Fig. 5 shows highlighted in green the undeformed geometry of the PDMS sample. After scaling and processing the photo, the real initial dimensions of the sample were measured. The sample had a length of $10[mm]$, a width of $3.465[mm]$ and a thickness of $100[\mu m]$ (the latter known from the spin-casting process). These values were the initial dimensions of the geometry used in the finite element analysis.

3.1.2   Boundary Conditions

In the simulation, the boundary conditions were set up in the same way as performed in the experiment, i.e. one of the sides was fixed, whereas a prescribed displacement in the x-direction (horizontal direction) was applied at the other one. The upper and lower sides were left free.

3.1.3 Mesh, Type and Numbers of Elements

As mentioned in subsection 1.3, in order to ease the solution when nearly incompressible materials are used, a mixed U-P (displacement-pressure) formulation was performed. The elements used in the simulation were of the lagrangian type with quadratic shape functions for the displacements and linear functions for the pressure.

The input data used in the simulation are summarized in the following table (Table 1), with the MR coefficients calculated as it was shown in 1.3.1.

PDMS Bulk Modulus (K) $[MPa]$	PDMS Density $[Kg/m^3]$	$C_{10}[MPa]$	$C_{01}[MPa]$
962	0.971	0.059754522	−0.018087855

Table 1: PDMS Subdomain Input Data – Mooney Rivlin Model

The PDMS subdomain was meshed using hexahedral elements; the numbers of elements was 270 and the total number of degrees of freedoms was 8911.

So as to validate the MR model, the linear elastic model for the PDMS sample was also simulated to check consistency at small strains. Table 2 shows the constants used in the linear elastic model.

PDMS Young's Modulus (E) $[MPa]$	PDMS Poisson's Ratio (*)	PDMS Density $[Kg/m^3]$
0.250	0.499957	0.971
(*): derived from Equation 16		

Table 2: PDMS Subdomain Input Data – Linear Elastic Model

A Young´s modulus of 0.250 [MPa] was used for the PDMS calculated from the experimental data by Tae Kyung Kim et.al. A Poisson´s ratio of 0.499957 was derived from equation 16. These values were the input data in the linear elastic simulation.

$$v = \frac{3K - E}{6K} \tag{16}$$

3.2 Optical Model

Optical simulation was performed in an optical ray tracing software for optical design and analysis. The main advantages of using such software are the reduction in time and costs needed to design the optical prototype and to find the convenient characterization setup.

The number of rays used in the ray-tracing simulation was $1x10^6$. The light was set as monochromatic, collimated and coherent. The wavelength of light source was $632.8[nm]$ in concordance with the laser used in the experimental setup. As the initial grating pitch in the optical simulation, we used the results obtained from the experimental optical characterization of the undeformed sample. In section 4 the procedure to calculate the pitch of the grating is explained. The dimensions were the same as those simulated in the mechanical model and the distances from light source to the sample and from the sample to the detector plane (image plane) were the same as in the experiment.

4 EXPERIMENTAL SETUP AND CHARACTERIZATION PROCEDURE

A transmission diffraction scenario was carried out to characterize the PDMS grating and its sensitivity with the prescribed strains. This characterization procedure is the key element in
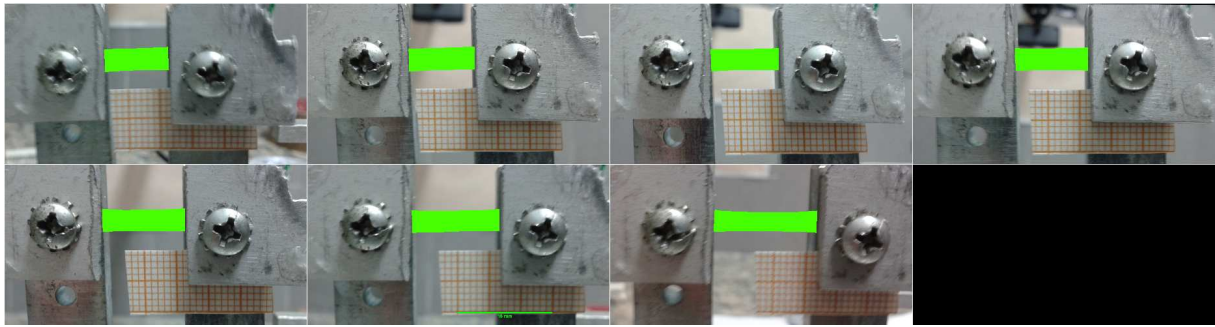
Figure 6: Photographic montage of the performed uniaxial tension test.

order to validate the use of the PDMS diffraction grating as a pressure sensor.

The PDMS strip is held by its ends in a homemade gripper as shown in Fig. 6. Highlighted in green is the PDMS sample; the sample is subjected to prescribed displacements and these are measured after postprocessing the photographs.

In subsection 1.2.1 , equation 1 gives the angles of the diffracted modes when a beam of monochromatic light pass through the diffraction grating. As said before, if the distance from the grating (sample) to the detector plane is much greater than the pitch of the grating, then the vertical distance of the mth-mode to the 0-mode is determined by equation 2.

Therefore, if the sample-detector distance D, the wavelength of light λ and the vertical distance of the mth mode are known, the pitch can be calculated. As it can be seen in the latter equation the vertical distance has a linear dependence on the diffraction-mode, so the vertical distances of the $[-2, -1, 0, +1, +2]$ modes were measured and a linear regression was made. Then, the slope and the pitch were calculated. In the next section, it is shown the linear regression made to estimate the pitch of the undeformed sample. This procedure was carried out with both the experimental results and those from simulation. In Fig. 7 it can be seen the diffraction pattern produced by the PDMS grating. The $[-2, -1, 0, +1, +2]$ modes are highlighted in green, whereas also the ±3 modes appear but attenuated. Below in the figure, the simulated diffraction pattern is shown with the distances between spots measured in pixels.

5 RESULTS AND DISCUSSION

The results in the work are first subdivided in those obtained from the mechanical analysis of the device and those attained from the optical simulation. It is also shown how the pitch of the grating was calculated in each case. At the end of this section, the results from the mechanical and optical models are coupled in order to compare them with the outcomes of the experiments.

5.1 Mechanical Model Results

The results of the mechanical model simulation are given in Fig. 8,Fig. 9 and Fig. 10. In the first figure it can be seen the three dimensional view of the sample when it was subjected to a prescribed displacement of $6[mm]$. These results correspond to the Mooney-Rivlin mechanical model. It was of interest to study the first principal stress field at the center of sample, where the grating was located; this is important to evaluate the uniformity of the strains produced in the region of interest (Fig. 8). In the second figure, the linear and non-linear mechanical models are compared. In addition, the experimental results achieved by Tae Kyung Kim et.al are shown. As it can be seen, there is consistency between the models and the experimental data in the range of small strains. For strains smaller than 0.35 the linear elastic model describes better the
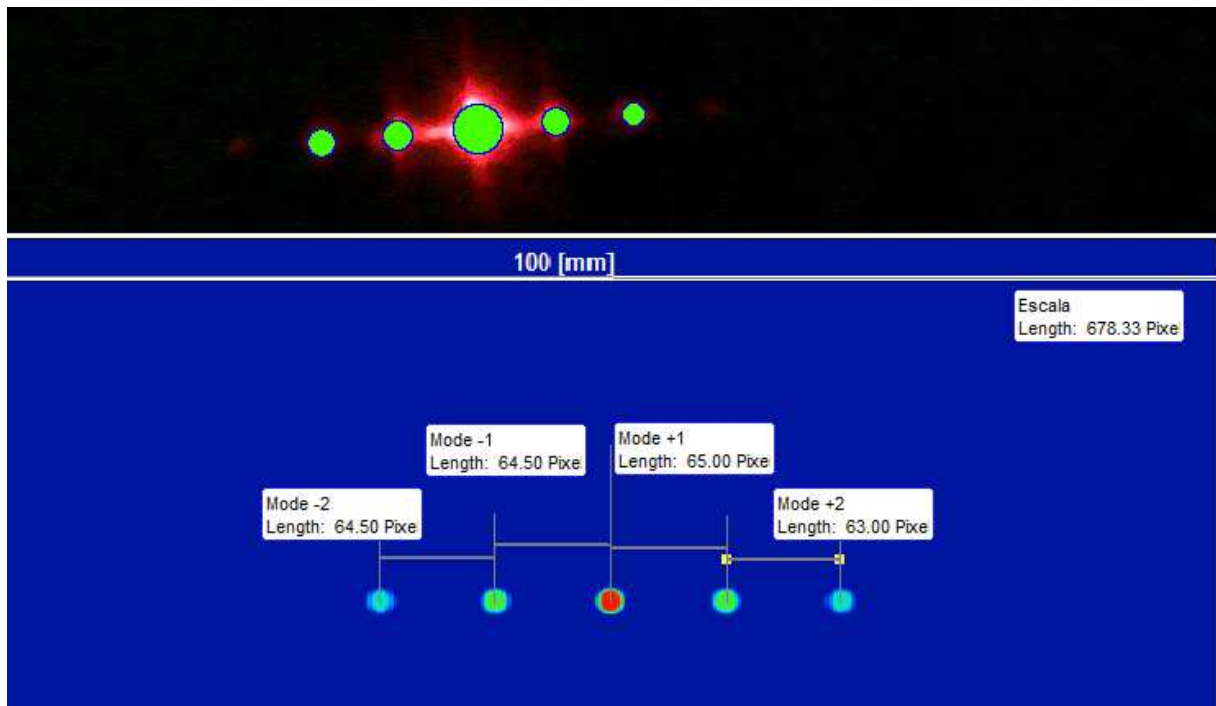
Figure 7: Diffraction pattern produced by the PDMS diffraction grating in the experiment (above) and the corresponding simulation (below).

stress-strain relationship, whereas for strains greater than 0.4 the MR model fits it better.
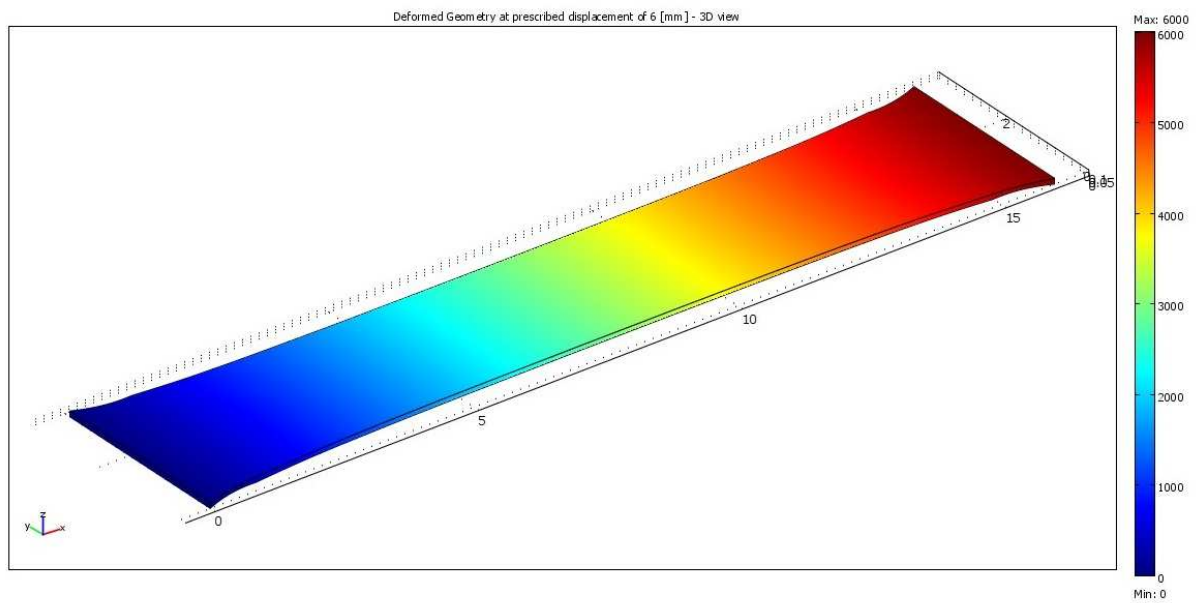
Figure 8: Three-dimensional view of the strained sample at a prescribed displacement of 6[mm].
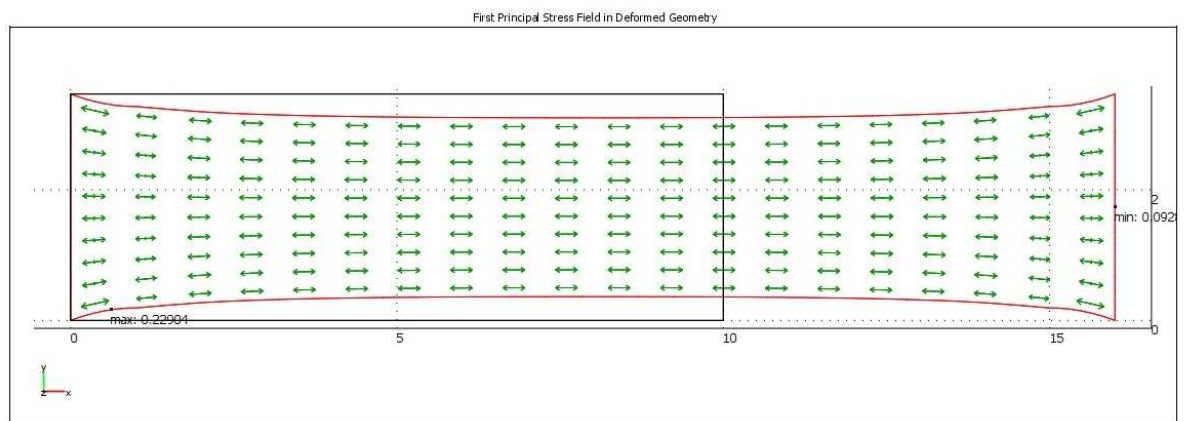

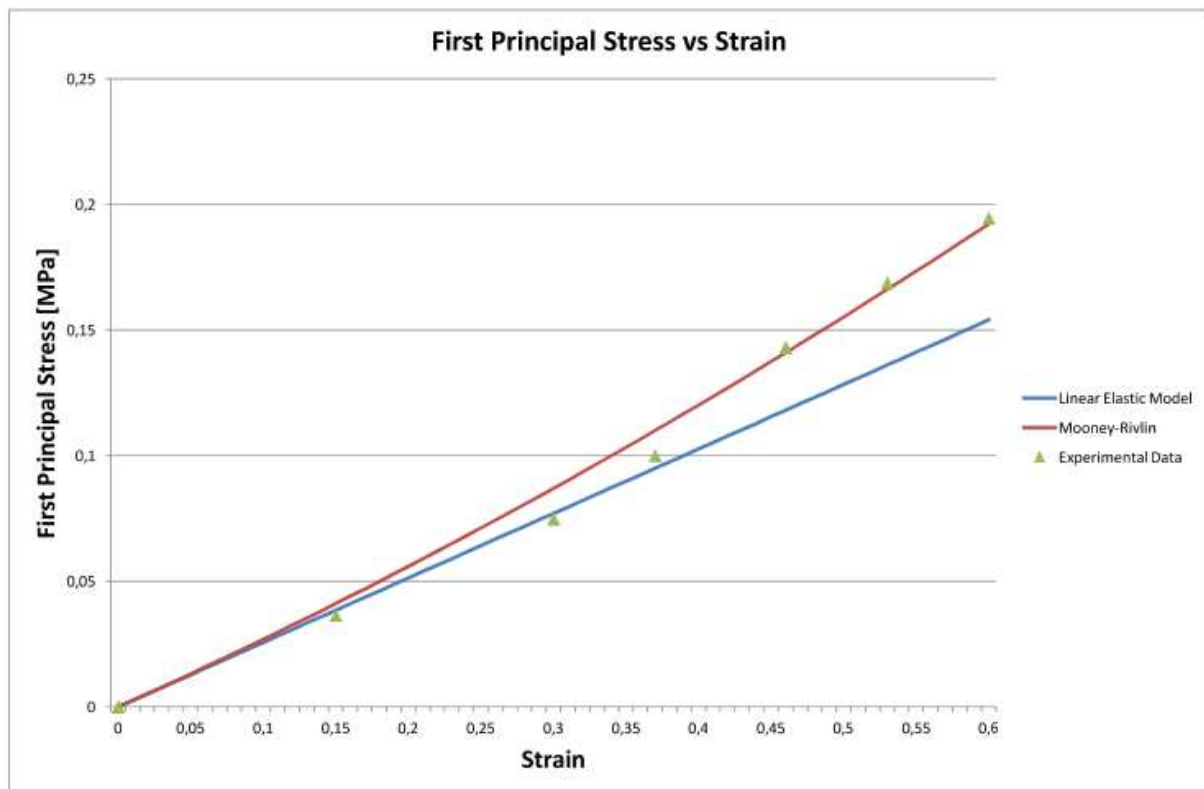Figure 9: First principal Stress Field of the deformed geometry (prescribed displacement of 6[mm]).

Figure 10: Stress-strain curves of the PDMS sample and comparison of the different models and the experimental data.

5.2   Optical Model Results

The optical simulations were performed with the assumptions made in 3.2. In Fig. 11 shows the procedure that was done in order to calculate the initial pitch value of the undeformed grating and the subsequent values as the sample was deformed. In the vertical axis the distances from each mode to 0-mode are shown; from the slope of the linear regression the pitch of the grating is calculated. The experimental data (green diamonds) are well-fitted with the linear regression (red dashed lines). This was the case for each estimation of the pitch values.

Fig. 12 shows a simulation of the diffraction grating for a particular pitch value (initial pitch in this case) with the consequent diffraction pattern; it is also displayed the distance from the sample to the detector. The color bar expresses the irradiance in $[W/cm^2]$.

5.3   Results from coupled models

After validation of the MR mechanical model, a parametric mechanical simulation was once again performed being the prescribed displacements-values in this case those measured from postprocessing of the experimental characterization photographs. The results are shown in Fig. 13 where a comparison between experiment a simulation is done. The variation of the pitch of the grating is displayed vs. the prescribed strain. The pitch varies from an initial value of $66[\mu m]$ in the undeformed geometry to an approximated final value of $114[\mu m]$ at a strain of around 0.63.
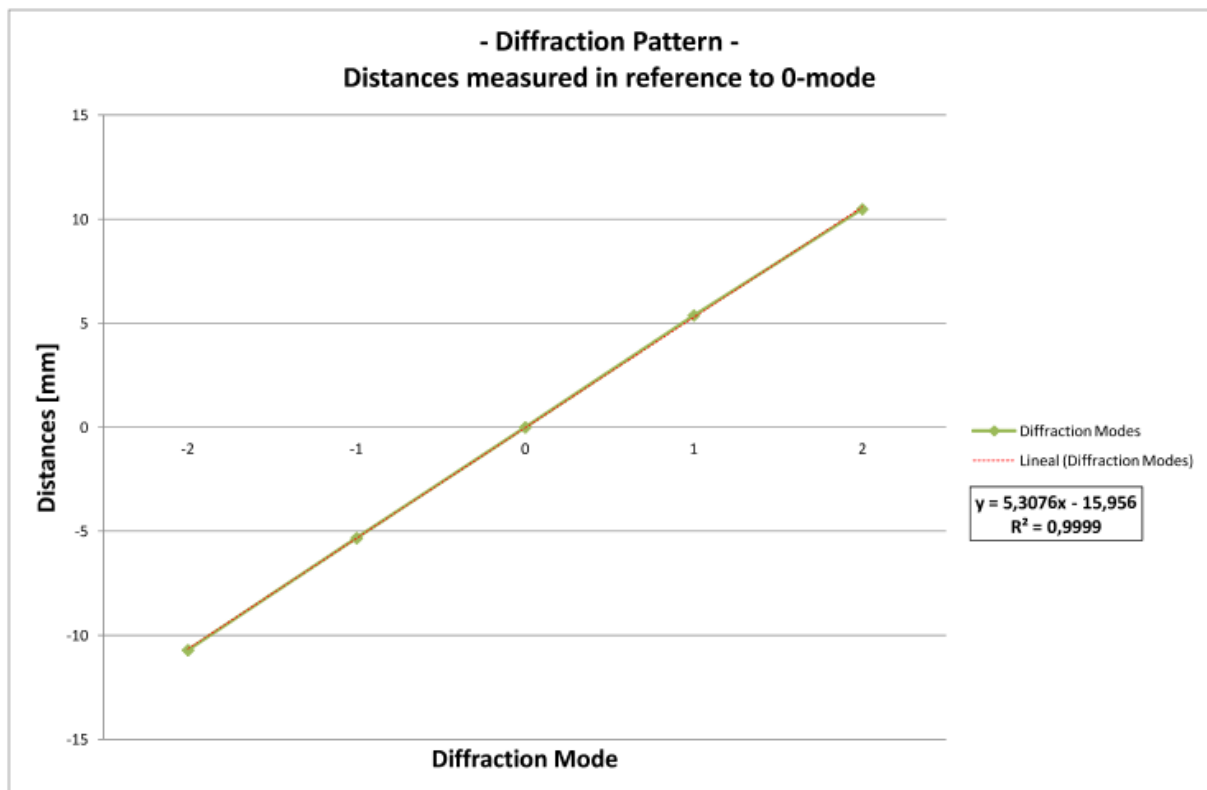
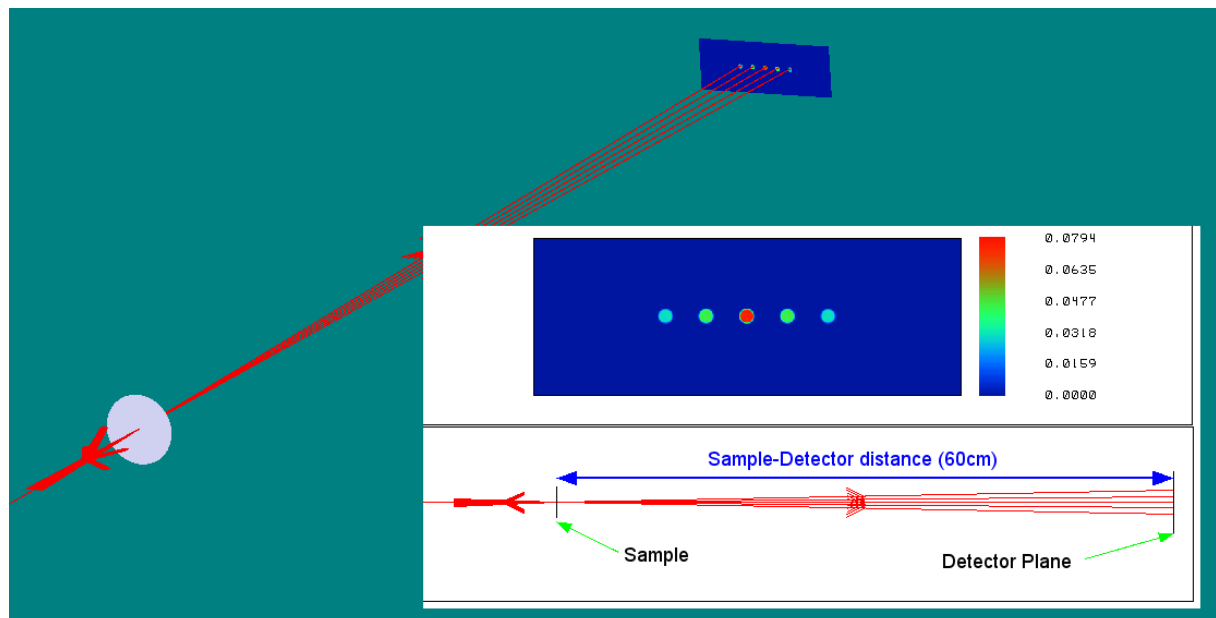Figure 11: Distances of the diffraction modes to 0-mode and the corresponding linear regression.

Figure 12: Simulation of the optical model, showing the diffraction pattern and the distance from sample to detector plane.
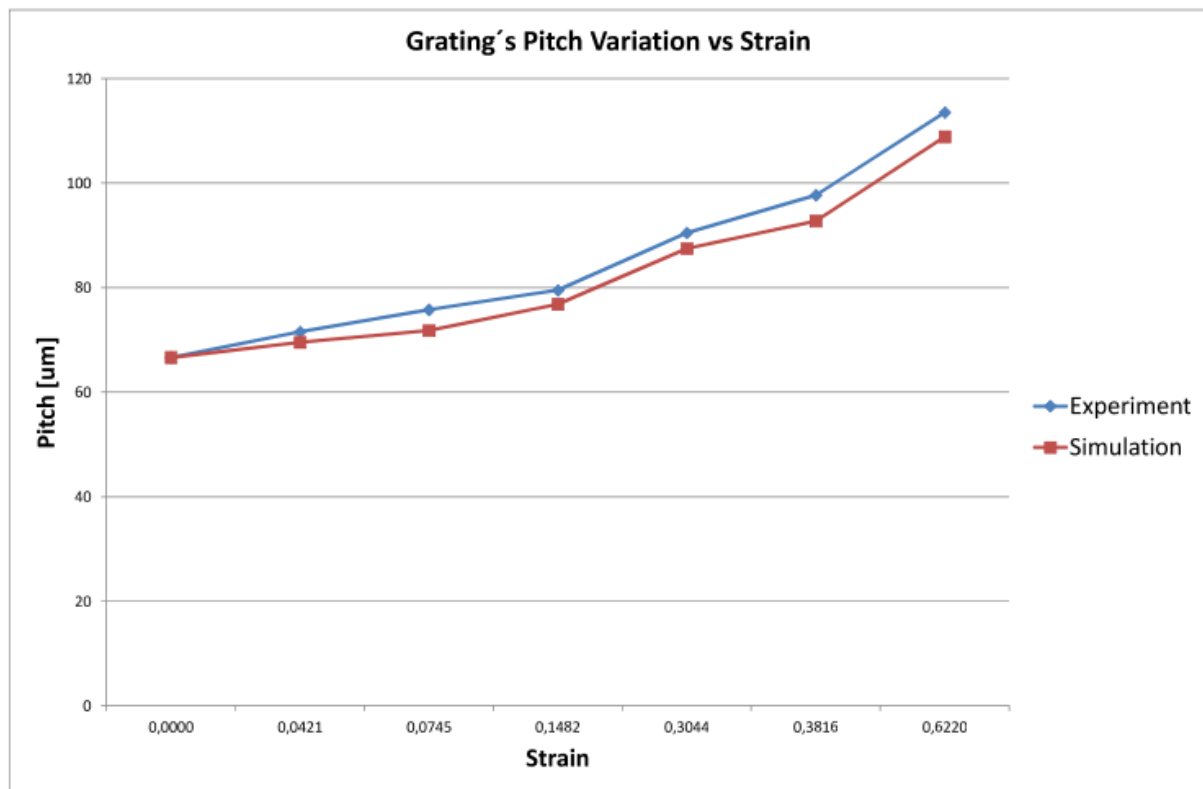
Figure 13: Comparison between experiment and the performed simulation using the Mooney-Rivlin model.

6 CONCLUSIONS

The design, fabrication and analysis of an optical passive microsensor have been presented in theory, simulation and experiment. The present work aimed to study the mechanical behavior of a PDMS diffraction grating, while also the variations in the optical properties of the grating, intended to be used as an optical passive microsensor. Therefore, a non-linear mechanical model (two parameters Mooney-Rivlin model) was used and compared with the linear elastic model so as to best describe the experimental results. The conclusion conducted by the finite element analysis showed that the non-linear model is better for modeling the stress-strain relationship of the sample in the desired entire range of strain. For more precise results other types of models, e.g. an Ogden or more parameters Mooney-Rivlin model have to be considered.

As intended, the device showed an optical response to mechanical deformations. From the findings presented here, it can be concluded that such a device can be used as pressure microsensor with the consequent benefits that it offers. The fabrication and characterization procedures were also presented and the results showed a good agreement between simulation and experiment with a relative good sensitivity. Of course, further analysis and simulations must be done: for example, it will probably be necessary to perform a biaxial extension test to completely describe the mechanical properties of the PDMS elastomer, and to use other mechanical models. Future work will focus on these aspects.

A pressure sensor based on PDMS diffraction grating was simulated. An opto-mechanical model was used in the pressure range of interest and resulted in a shift in the angular positions of light beams diffracted from the grating. From the analyses made, pitch variation was demonstrated. The sensitivity to changes in the radius of curvature was considered. Because the

probing beam was aimed at the center of the membrane, there were no considerable variations in the position of the diffracted beams. The variations in the pitch due to mechanical deformation produced sufficient optical response to applied pressure ranging from 0 to 2500[Pa].

7 ACKNOWLEDGEMENTS

REFERENCES

Braggio L. and Guarnieri F. Mecánica computacional, volume xxxi. number 24. computational modeling in bioengineering and biomedical systems (a). ????

Chronis N., Liu G., Jeong K., Lee L., et al. Tunable liquid-filled microlens array integrated with microfluidic network. *Opt. Express*, 11(19):2370–2378, 2003.

Corning D. Sylgard 184 silicone elastomer - datasheet, month = jul, year = 2011, url = http://www.dowcorning.com/. ????

Dong Y., Lin R., and Bhattacharyya D. Determination of critical material parameters for numerical simulation of acrylic sheet forming. *Journal of materials science*, 40(2):399–410, 2005.

Foland S., Liu K., MacFarlane D., and Lee J. High-sensitivity microfluidic pressure sensor using a membrane-embedded resonant optical grating. In *Sensors, 2011 IEEE*, pages 101–104. IEEE, 2011.

Grayson A.R., Shawgo R.S., Johnson A.M., Flynn N.T., Li Y., Cima M.J., and Langer R. A biomems review: Mems technology for physiologically integrated devices. *Proceedings of the IEEE*, 92(1):6–21, 2004.

Hecht E. Optics. 4th. 2002.

Hosokawa K. and Maeda R. In-line pressure monitoring for microfluidic devices using a deformable diffraction grating. In *Micro Electro Mechanical Systems, 2001. MEMS 2001. The 14th IEEE International Conference on*, pages 174–177. IEEE, 2001.

Keum H., Carlson A., Ning H., Mihi A., Eisenhaure J., Braun P., Rogers J., and Kim S. Silicon micro-masonry using elastomeric stamps for three-dimensional microfabrication. *Journal of Micromechanics and Microengineering*, 22(5):055018, 2012.

Kim T.K., Kim J.K., and Jeong O.C. Measurement of nonlinear mechanical properties of pdms elastomer. *Microelectronic Engineering*, 88(8):1982–1985, 2011.

Palmer C. and Loewen E. *Diffraction grating handbook*. Newport Corporation, 2005.

Schueller O., Duffy D., Rogers J., Brittain S., and Whitesides G. Reconfigurable diffraction gratings based on elastomeric microfluidic devices. *Sensors and Actuators A: Physical*, 78(2):149–159, 1999.

Wilbur J., Jackman R., Whitesides G., Cheung E., Lee L., and Prentiss M. Elastomeric optics. *Chemistry of materials*, 8(7):1380–1385, 1996.

Xia Y. and Whitesides G.M. Soft lithography. *Annual review of materials science*, 28(1):153–184, 1998.

Yoon S., Reyes-Ortiz V., Kim K., Seo Y., and Mofrad M. Analysis of circular pdms microballoons with ultralarge deflection for mems design. *Microelectromechanical Systems, Journal*

of, 19(4):854–864, 2010.

Yu Y. and Zhao Y. Deformation of pdms membrane and microcantilever by a water droplet: Comparison between mooney-rivlin and linear elastic constitutive models. *Journal of colloid and interface science*, 332(2):467–476, 2009a.

Yu Y.S. and Zhao Y.P. Deformation of pdms membrane and microcantilever by a water droplet: Comparison between mooney–rivlin and linear elastic constitutive models. *Journal of colloid and interface science*, 332(2):467–476, 2009b.